Diurnal Cycles of Synthetic Microwave Sounding Lower-Stratospheric Temperatures from Radio Occultation Observations, Reanalysis, and Model Simulations

AODHAN J. SWEENEY[a] AND QIANG FU[a]

[a] *University of Washington, Seattle, Washington*

(Manuscript received 25 May 2021, in final form 19 October 2021)

ABSTRACT: An observationally based global climatology of the temperature diurnal cycle in the lower stratosphere is derived from 11 different satellites with global positioning system–radio occultation (GPS-RO) measurements from 2006 to 2020. Methods used in our analysis allow for accurate characterization of global stratospheric temperature diurnal cycles, even in the high latitudes where the diurnal signal is small but longer time-scale variability is large. A climatology of the synthetic Microwave Sounding Unit (MSU) and Advanced MSU (AMSU) Temperature in the Lower Stratosphere (TLS) is presented to assess the accuracy of diurnal cycle climatologies for the MSU and AMSU TLS observations, which have traditionally been generated by model data. The TLS diurnal ranges are typically less than 0.4 K in all latitude bands and seasons investigated. It is shown that the diurnal range (maximum minus minimum temperature) of TLS is largest over Southern Hemisphere tropical land in the boreal winter season, indicating the important role of deep convection. The range, phase, and seasonality of the TLS diurnal cycle are generally well captured by the WACCM6 simulation and ERA5 dataset. We also present an observationally based diurnal cycle climatology of temperature profiles from 300 to 10 hPa for various latitude bands and seasons and compare the ERA5 data with the observations.

KEYWORDS: Remote sensing; Sampling; Satellite observations

1. Introduction

Temperature diurnal cycles of the lower stratosphere result from atmospheric absorption of both short and long wave radiation leading to interactions between migrating and nonmigrating tides (Chapman and Lindzen 1970). Because of the complexity of the temperature diurnal cycle, it can provide a helpful test in assessing a model's depiction of the atmosphere (Dai and Trenberth 2004). In the tropics, the upper-tropospheric–lower-stratospheric (UTLS) temperature diurnal cycle has been found to be strongly influenced by the diurnal cycle of deep convection which may have implications for the hydration of the stratosphere (Khaykin et al. 2013; Johnston et al. 2018). Temperature diurnal cycles in this region have also been shown to be potentially related to high-frequency stratospheric–tropospheric exchange through their influence on the diurnal variability of the cold-point tropopause (Suneeth et al. 2017).

Documentation of diurnal cycles in this region is also important for estimation of decadal temperature trends in the lower stratosphere. Long-term temperature records obtained by the Microwave Sounding Unit (MSU) and Advanced MSU (AMSU) may alias in diurnal temperature cycles because of the diurnal drift experienced by the satellites carrying the MSU and AMSU (Mears et al. 2003). To correctly account for this spurious diurnal signal, a reliable diurnal cycle must be documented for the layers that MSU and AMSU are sampling. These issues motivate our study to document the lower-stratospheric temperature diurnal cycles.

One of the first studies attempting to document stratospheric temperature diurnal cycles used radiosonde data from various locations in the Northern Hemisphere but found that stratospheric temperature data from radiosondes were not suited to derive reliable diurnal cycles there (Seidel et al. 2005). Other studies have used global positioning system–radio occultation (GPS-RO) data to document the migrating and semidiurnal tide in the stratosphere but because of insufficient sampling and large atmospheric variability, these studies have been confined to lower latitudes (Zeng et al. 2008; Pirscher et al. 2010; Xie et al. 2010).

The most salient problem in deriving a diurnal cycle climatology is the incomplete sampling of all local time hours in a given region. This occurs because satellites tend to sample at specific local times due to their orbital configuration, leading to gaps in the diurnal cycle (Pirscher et al. 2007). Another closely related challenge is how to remove the impact of large background temperature variability on the derived diurnal cycles, especially over the high latitudes (Pirscher et al. 2007). Because of these challenges, many studies attempting to document stratospheric temperature diurnal cycles have been limited in their latitudinal coverage (Pirscher et al. 2007, 2010; Xie et al. 2010). Pirscher et al. (2010) provided an effective method for removing atmospheric variability with time scales greater than one day using a European Centre for Medium-Range Weather Forecasts (ECMWF) forecast but was unable to provide confident measurements at latitudes higher than 50°. Previous studies have also relied on spectral methods or harmonic decomposition to measure the diurnal and semidiurnal tides, neglecting higher-order and longitudinal variations. To derive a global stratospheric temperature diurnal cycle climatology, especially over high latitudes, more samples with several orbital configurations are needed.

Full diurnal sampling at most latitudes can be achieved with approximately one month of the Constellation

Corresponding author: Aodhan Sweeney, aodhan@uw.edu

DOI: 10.1175/JTECH-D-21-0071.1

Observing System for Meteorology, Ionosphere and Climate (COSMIC) (Pirscher et al. 2010) but much longer time periods using only polar-orbiting radio occultation satellites (Zeng et al. 2008). Attempting to create a diurnal cycle climatology using too few samples may alias significant errors from changes in background temperature. This is particularly true at high latitudes in winter where atmospheric variability is largest. Some studies have had success in characterizing the diurnal cycles in the tropical UTLS where atmospheric variability is small. These studies have found diurnal ranges of 1–2 K for the migrating tide near 30 km and slightly lower diurnal ranges near the tropical tropopause (e.g., Zeng et al. 2008; Xie et al. 2010; Khaykin et al. 2013; Suneeth et al. 2017; Das et al. 2020).

The primary goal of this study is to provide a diurnal cycle climatology of the MSU and AMSU Temperature in the Lower Stratosphere (TLS) to assess model and reanalysis-based diurnal cycle climatologies used for the diurnal correction. MSU/AMSU satellite observations are critical for quantifying multidecadal tropospheric warming and stratospheric cooling (e.g., Christy et al. 2000; Mears et al. 2003; Fu and Johanson 2004; Fu et al. 2004, 2006, 2010; Fu and Lin 2011; Fu et al. 2011; Mears and Wentz 2016; Santer et al. 2017, 2019; Po-Chedley et al. 2021). In deriving multidecadal temperature trends, a primary source of uncertainty comes from local time sampling changes resulting from satellite orbital diurnal drift (e.g., Mears et al. 2002; Fu and Johanson 2005; Mears and Wentz 2005; Wentz and Schabel 1998). This change in local time sampling contaminates satellite-derived climate trends by aliasing diurnal cycles of temperature into MSU/AMSU observations. To achieve a reliable long-term temperature record, corrections accounting for the diurnal drift must be applied. Diurnal contamination is largest for MSU/AMSU channels that peak near Earth's surface because conduction from Earth's surface heats air close to the ground efficiently over land, along with the direct emission contribution from the surface. Other studies have examined diurnal cycle climatologies of surface and tropospheric temperatures, but fewer have tried to characterize the upper-air temperature diurnal cycles like the TLS channel (Mears et al. 2003; Mears and Wentz 2005; Kennedy et al. 2007; Po-Chedley et al. 2015).

Different methods have been developed to account for satellite diurnal drift. Some have used the output of the Community Climate Model (CCM3) GCM to estimate the diurnal corrections (Mears et al. 2003; Mears and Wentz 2005; Zou and Wang 2009). Mears et al. (2011) quantified the uncertainty associated with this technique based on a Monte Carlo method and showed that almost one-third of the uncertainty in the TLS multidecadal temperature trend was due to the diurnal drift correction, and even higher values for other channels. Because of the limited number of models used in this study, this may still be an underestimate. A more recent study has used the MSU/AMSU data to derive an observationally based diurnal correction for the midtroposphere temperature (Po-Chedley et al. 2015). Using this observationally based diurnal correction, Po-Chedley et al. (2015) showed that tropical tropospheric warming patterns have higher consistency with GCM warming patterns when compared to using GCM-based diurnal corrections. An earlier study showed that diurnal climatologies derived from GCMs have biases (Dai and Trenberth 2004), specifically the CCSM2. Ideally, an observationally based temperature record with a high accuracy could be used to derive diurnal cycle climatologies and evaluate GCM simulations (Mears et al. 2011; Mears and Wentz 2016).

GPS-RO data provide temperature observations with a high vertical resolution and accuracy in the UTLS (Kursinski et al. 1997), approximately near the peak of the TLS weighting function, making GPS-RO a prime candidate to derive a TLS diurnal cycle climatology. Using over 14 years of radio occultation data from 11 different satellite systems stored at the COSMIC Data Analysis and Archive Center (CDAAC) at the University Center for Atmospheric Research, we compute a global TLS channel diurnal cycle climatology as well as a lower stratospheric temperature profile diurnal cycle climatology from 300 to 10 hPa. We use the TLS diurnal cycles derived from radio occultation measurements to check those from GCM and reanalysis data to evaluate the skill of previous TLS diurnal cycle climatologies based on GCMs alone. Section 2 describes the data used in this study. Section 3 examines the GPS-RO sampling characteristics and describes the data compositing methods, and section 4 presents the global climatologies derived from GPS-RO observations and their comparisons with reanalysis and model simulations. The conclusions are given in section 5.

2. Data

a. GPS-RO

We use radio occultation data from the CDAAC at the University Center for Atmospheric Research. Radio occultations are retrieved using an active limb sounding technique, allowing for retrieval of bending angle and refractivity, which can be used to derive temperature (Kursinski et al. 1997). GPS-RO temperature profiles have high accuracy (less than 0.1 K), as well as high vertical resolution (~0.5 km, but can vary based on latitude) in the UTLS, but coarser horizontal resolution (about 200 km) (Kursinski et al. 1997; Kuo et al. 2004; Zeng et al. 2019). Validation efforts have shown that the results of COSMIC are in good agreement with radiosonde data, especially for temperature profiles (He et al. 2009; Zeng et al. 2019). We use the level-2 wetPrf product which provides estimates of temperature including the effects of moisture. Temperatures from the wet and dry profiles converge when humidity is negligible (as it is in the UTLS), or at temperatures less than 250 K (Kursinski et al. 1997). WetPrf latitude and longitude information from the occultation is attained by using the 17.4-km tangent point (near the peak of the TLS weighting function), local time is then obtained using the time stamp and longitude of the profile (Young et al. 2012). The CDAAC provides profiles with temperature every 100 m. We use temperature information provided between 8 and 40 km to characterize the TLS diurnal cycle.

TABLE 1. Periods of data used from each satellite, the average amount of radio occultations per day, and the mean difference as compared to *MetOp-A*. The number of collocations used to compute the mean difference is also included. The mean difference and number of samples with two values represent reprocessed data (R) and postprocessed data (P). Samples per day is calculated by taking the total amount of samples and dividing by the number of days in the period column.

Satellite	Period	$\mu_{\text{difference}}$	No. of collocations	Samples per day
COSMIC-1	June 2006–May 2020	0.0085/0.0114	15 606/5972	1204
COSMIC-2	October 2019–November 2020	−0.1535	6414	3860
GRACE	March 2007–November 2017	0.0454	2310	135
KSAT-5	January 2015–November 2020	0.0520	1797	256
MetOp-A	October 2007–November 2020	−0.0320/−0.0207	6552/3138	586
MetOp-B	February 2013–November 2020	−0.0056/−0.0150	6294/1831	575
MetOp-C	July 2019–November 2020	−0.0263	1878	552
PAZ	May 2018–November 2020	−0.0296	648	187
SAC-C	March 2006–August 2011	−0.0147	1576	194
TDX	January 2016–November 2020	0.0330	1048	151
TSX	February 2008–November 2020	0.0091	2654	174

Radio occultation data from the CDAAC comes in various processing levels: near–real time (NRT), postprocessed (PP), and reprocessed (RP). CDAAC recommends that RP data be used first, then PP and NRT. RP data are infrequently updated and only available for *COSMIC-1*, *MetOp-A*, and *MetOp-B*. The only satellite from which we use NRT data is *COSMIC-2*, for which PP and RP data have not been released. We use over 14 years of GPS-RO data from 11 different satellites from March 2006 to November 2020 (Table 1), collecting over 13 million occultation measurements in total.

To provide uncertainty estimates for the GPS-RO derived diurnal cycle, we perform a 10 000-iteration bootstrap and calculate a $\pm 2\sigma$ estimate of the diurnal anomaly at each time bin. This is done by first splitting the date into seasons, there are 42 months of processed data for DJF and 45 for MAM, JJA, and SON. For each iteration of the bootstrap, we randomly select a set of N months for each season with replacement where N is the total amount of months of data in that season (e.g., for DJF $N = 42$). This provides 10 000 different versions of the diurnal cycles for each season and allows for estimation of the diurnal anomalies' confidence intervals.

b. ERA5

ERA5 is the most recent generation of reanalysis data provided by ECMWF. ERA5 has many improvements over the previous generation of reanalysis data (ERA-Interim) including a higher horizontal native resolution (0.25°) and a near doubling of the vertical resolution in the UTLS region. ERA5 is based on the Integrated Forecasting System by ECMWF (Hersbach et al. 2020). ERA5 data have been significantly aided by the assimilation of radio occultation data, which began in 2006 (Hersbach et al. 2020).

We use ERA5 hourly temperature reanalysis data on pressure levels from 2006 to 2020 on a 0.25° latitude × 0.25° longitude grid with 20 pressure levels from 350 to 2 hPa. We then interpolate every temperature profile in the record to 320 vertical levels to match that of the radio occultation spacing (which spans 8–40 km with 100-m vertical spacing, as stated above).

c. WACCM6

The Whole Atmosphere Community Climate Model version 6 (WACCM6) is the latest version of the Community Earth System Model with major updates in the physical and chemical representation of our atmosphere (Gettelman et al. 2019). We use five years of hourly output from a WACCM6 modern climate simulation (Fu et al. 2020) to document the diurnal cycles in TLS temperature. WACCM6 data are output on a 0.9° × 1.25° latitude by longitude grid, with 28 pressure levels between 350 and 2 hPa. These data are also interpolated to 320 levels to match that of the radio occultation data.

d. CCM3

The AMSU channel 9 diurnal cycle climatology derived using CCM3 is provided by the Remote Sensing Systems (ftp://ftp.remss.com/msu/data/diurnal_cycle/) for each view angle. We compare the CCM3 AMSU channel 9 TLS diurnal cycles to our results from the GPS-RO, ERA5, and WACCM6 data. Diurnal cycles for GPS-RO, ERA5, and WACCM6 datasets are created using the MSU channel 4 weighting function. Mears and Wentz (2009) found that there is a difference of ~0.5 km in the height of the weighting function for the nadir MSU channel 4 and near-nadir AMSU channel 9. To correct for this difference peak weighting function height, Mears and Wentz (2009) recommended using a combination of AMSU channel 9 view angles 7–10 and 21–24 to create a weighting function which more closely matched that of MSU channel 4. We thus use a combination of CCM3 diurnal cycles recommended by Mears and Wentz (2009) to account for differences in the weighting function. The RSS CCM3 AMSU-9 near-nadir diurnal cycle is a 5-yr climatology for all months and has a horizontal resolution of 2.5° latitude × longitude.

e. TLS weighting function

The MSU channel 4 weighting function is publicly available from NOAA/Center for Satellite Applications and Research (STAR) (ftp://ftp.star.nesdis.noaa.gov/pub/smcd/emb/mscat/data/AMSU/AMSU_v2.0/AMSUA_only_Monthly_Layer_Temperature/Weighting_Function/). The analogous channel on AMSU is channel 9; together these channels represent the MSU/AMSU

TLS channel. The TLS weighting function peaks at 17.4 km, but its tails extend from 3 to 60 km. We consider the vertical range from 8 to 40 km by renormalizing the weighting function to its integration between 8 and 40 km. This renormalized weighting function allows us to compute the synthetic TLS temperatures from the GPS-RO, ERA5, and WACCM6 data consistently.

3. Deriving the global TLS diurnal cycle climatology from GPS-RO

Overcoming biases from incomplete diurnal sampling is the biggest hurdle in deriving a global diurnal cycle climatology from GPS-RO data. To overcome sampling biases, we use data from several satellites for many years. Radio occultations do not need calibration and thus there should be little to no intersatellite bias (Anthes et al. 2008; Ho et al. 2009; Anthes 2011). To confirm that data used have small intersatellite biases, we perform collocations between each satellite used in the study and a reference satellite. In this context, collocations are defined as occultations occurring within three hours and in the same 1.5° × 1.5° grid cell. We then take the difference between the TLS obtained by a given satellite and the reference. If collocated intersatellite biases are small, then we expect that the mean differences are close to zero. *MetOp-A* is chosen as the reference satellite because it has been operational for nearly the entire period considered, thus all other satellites can be compared to *MetOp-A*. The mean difference ($\mu_{\text{difference}}$) is given in Table 1. Because *MetOp-A*, *MetOp-B*, and *COSMIC-1* have two different data processing levels (RP and PP), there are two $\mu_{\text{difference}}$ corresponding to the mean difference for RP and PP data. We also include the $\mu_{\text{difference}}$ between the collocations of *MetOp-A* to itself to provide a reference in which to compare the magnitudes of the mean differences. The mean difference ($\mu_{\text{Difference}}$) magnitudes are generally smaller than ~0.05 K except for *COSMIC-2* that has a mean difference magnitude of ~0.15 K. This relatively large mean difference has little impact on our results; when we calculate the diurnal cycle after removing the $\mu_{\text{Difference}}$ between *MetOp-A* and *COSMIC-2* from all *COSMIC-2* occultations we found negligible difference in the constructed diurnal cycles (not shown). The samples/day category is the total number of samples divided by the number of days that each satellite was in operation. It should be noted that the samples per day of a given satellite can vary throughout the time of operation of a given satellite, especially *COSMIC-1*, which had nearly ~2500 samples per day in 2006, but ~250 samples per day in 2019.

a. Sampling characteristics

Most GPS-RO satellites used in this study are polar orbiting and thus the ascending and descending paths typically observe the same respective local times each day. Because of their near stationary precession relative to Earth, polar-orbiting satellites are ill equipped to derive a diurnal climatology on their own. Further, polar observations from any one satellite system suffer from the fact that ascending and descending tracks converge near the poles, so ascending and descending measurements are close in time. Higher precession rates of the constellation systems are necessary to resolve this issue. Because constellation systems are also composed of several satellites separated by a given phase, full diurnal sampling is achieved even faster. Although the constellations are much better at reaching full diurnal sampling, their observations of the poles are less frequent than their observations of the midlatitudes and subtropics because of their lower orbital inclination.

Although one polar-orbiting satellite on its own cannot achieve a full diurnal sampling, more local times can be sampled by using all polar-orbiting satellites. This has the added benefit of more frequent high latitude measurements in our attempt to characterize the TLS diurnal cycle near the poles. By using all available polar-orbiting RO satellites in tandem with the constellation systems from *COSMIC-1* and *COSMIC-2*, we can achieve sufficient local time sampling to characterize TLS diurnal cycles over the globe. Figure 1 shows the number of samples taken in one month as a function of local time and latitude for each satellite considered in this study. Constellation systems (*COSMIC-1* and *COSMIC-2*) show dense sampling at all local times but only at certain latitudes, while polar-orbiting satellites can sample almost all latitudes but only at certain local times. Higher density sampling occurs near 20° and 60° where ascending and descending orbital tracks meet. Polar-orbiting satellites have similar local time sampling within one month but slight differences in the orbital geometry of each satellite allow for enhanced diurnal sampling when all satellites are composited.

Figure 2 shows the evolution of composite sampling distribution throughout the record. As satellites are phased in and out of operation, the sampling characteristics for each month of the composite change. The composite of all GPS-RO data over 14 years thus enables us to sample local times that may be missed on shorter time scales with fewer satellites. The full composite of all GPS-RO data separated by season, 3-h local time bin, and 10 latitudinal bands is provided in Fig. 3. This composite includes more than 13 million observations. The zonal bands are chosen to have sufficient sampling to create a reliable climatology, as well as having approximately equal area. The bands are equator–10°, 10°–20°, 20°–40°, 40°–60°, and 60°–90°. Like Fig. 1, the highest density sampling is where the ascending and descending orbital tracks meet.

b. Compositing GPS-RO data

Satellite derived climatologies of diurnal cycles involve averaging multiple observations from many years over the same local time. This climatology has no confounding assumptions but is heavily dependent on complete diurnal sampling and the variability of the synoptic environments which are being sampled (Pirscher et al. 2010). Aliasing errors may arise in the derived climatology by averaging data at the same local time hour over many different synoptic environments, thus incorporating background changes of temperature into the diurnal cycle. Aliasing errors are thus largest when atmospheric

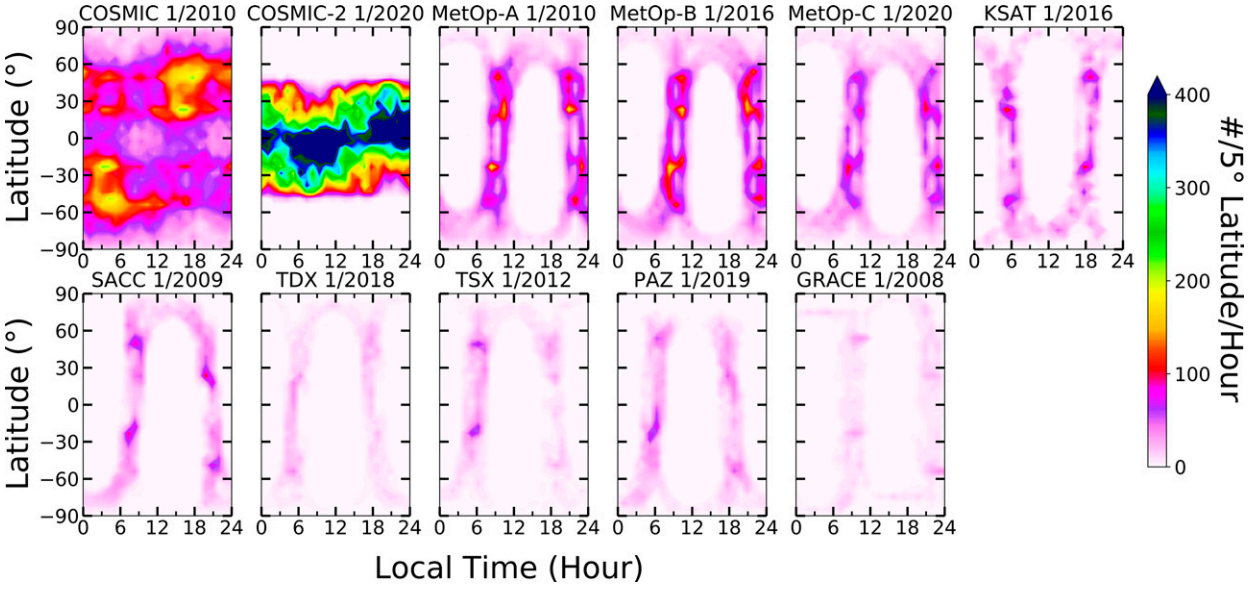

FIG. 1. Sampling frequency (number per month) as a function of local time and latitude during one January for each GPS-RO satellite. Occultations are binned into a 5° latitude zonal band and 1-h local time bin.

variability is highest, namely, in the high-latitude winter and spring (e.g., Pirscher et al. 2007, 2010).

To reduce such errors, every occultation is first binned into a 5° latitude × 10° longitude box. This is done for each day in the record. The daily mean TLS is derived from ERA5 by averaging over all local time hours for each day over the same box. This average is then removed from all GPS-RO derived TLS measurements in each box. This step reduces aliasing errors by removing changes in background temperature associated with variability of time scales longer than 1 day. A similar technique was used in Pirscher et al. (2010) to characterize the migrating tide from 50°S to 50°N. Here we use latitudinally and longitudinally (i.e., every 5° × 10°) varying daily mean removals. We also use data from 11 satellites over 14 years to maximize the number of observations at different local time hours in order to characterize the diurnal cycles over the globe. Occultations are then composited into 3-h local time bins (centered at 0130, 0430, …, and 2230 local time).

Removing the daily mean from each occultation in the 5° × 10° box with ERA5 might incorporate bias into our climatology. This is due to potential temperature bias present in the

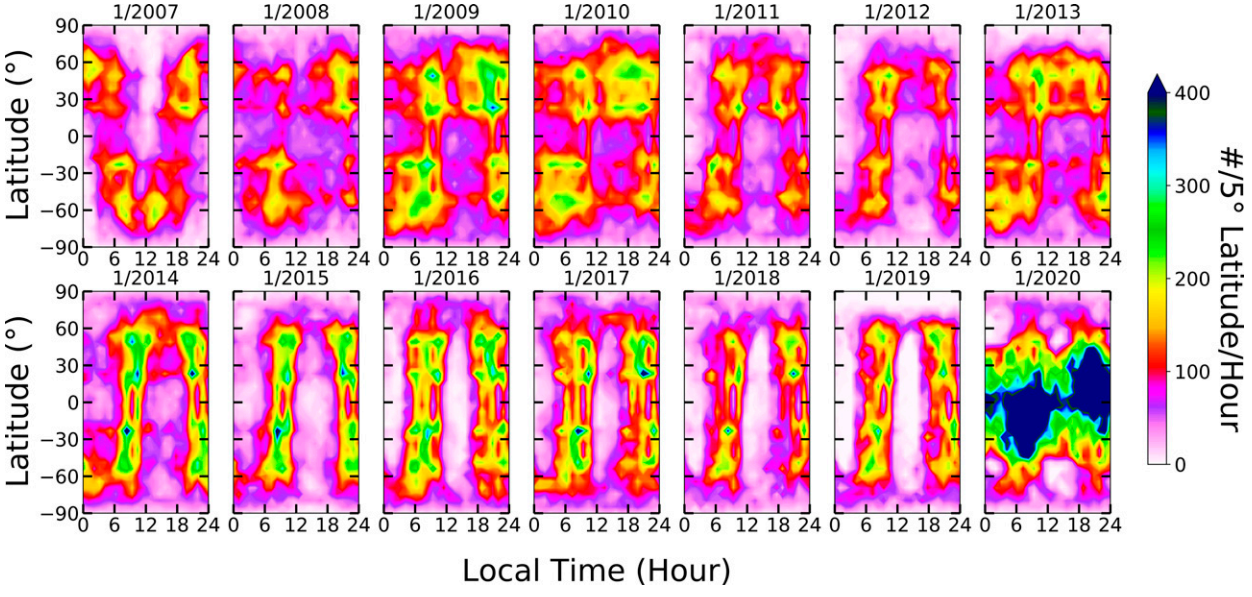

FIG. 2. As in Fig. 1, but for 1-month composites of all GPS-RO data available for each January from 2007 to 2020.

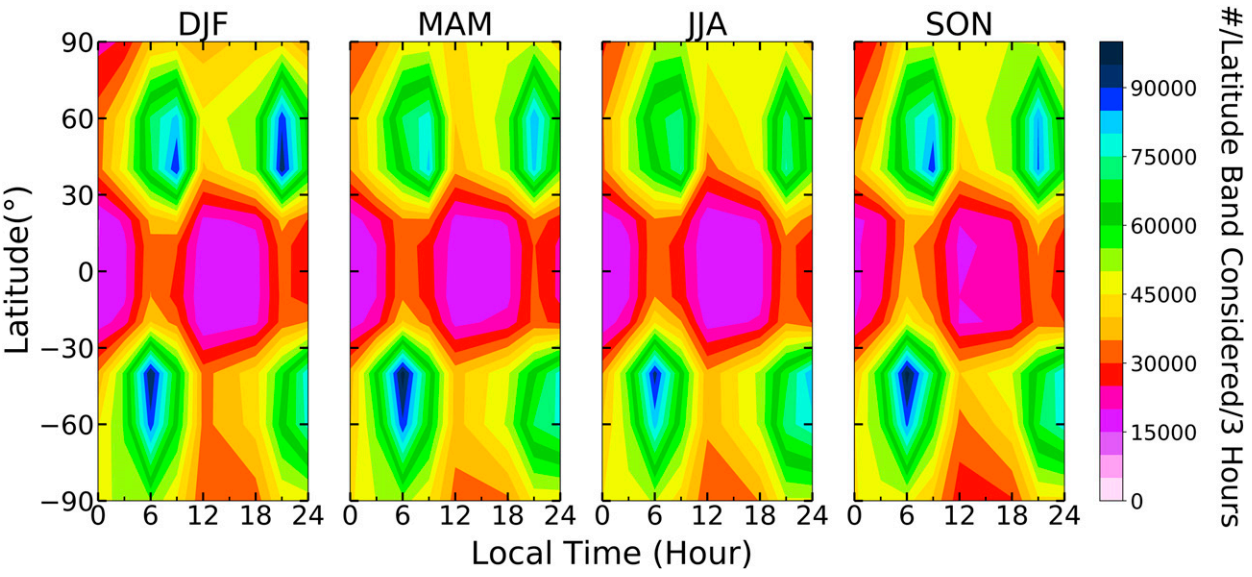

FIG. 3. Sampling frequency (number per season) of GPS-RO observations using all satellites and all years. Occultations are binned into 10 latitudinal bands for every 3-h local time bin. The latitudinal bands are 0°–10°N/S, 10°–20°N/S, 20°–40°N/S, 40°–60°N/S, and 60°–90°N/S.

ERA5 data (Simmons et al. 2020). For example, near the peak of the TLS weighting function ERA5 has a cold bias. We attempt to reduce this bias by subtracting the mean of the GPS-RO composite diurnal cycle in each 5° × 10° box after ERA5 daily means are removed (residual mean removal). We choose one month in order to have sufficient diurnal sampling to estimate the mean of the diurnal cycle.

After removing the daily mean ERA5 and the monthly residual mean from each 5° × 10° box, we then take an area weighted average of all boxes in every zonal band for each season and every 3-h local time interval. See Fig. 3 for the sampling frequency distribution for such composite. Using the techniques presented above, smaller regions than the zonal bands used here (including longitudinally varying regions) can be considered in the midlatitudes and tropics. A schematic flowchart describing the above steps to create the diurnal cycle climatology from GPS-RO measurements is provided in Fig. 4.

The reduction in aliasing errors after removing the daily mean and monthly mean residual is checked by using collocated ERA5 temperatures, i.e., the ERA5 TLS at the closest latitude, longitude, and local time hour for each radio occultation in the record. Because this set of collocations contains the same sampling characteristics as the GPS-RO data, it can be used to quantify aliasing errors by comparing diurnal cycles generated from the collocated dataset to those generated from the full ERA5 dataset.

Figure 5 shows the TLS diurnal cycles for the 10 zonal bands and 4 seasons using the full ERA5 dataset from 2006 to 2020 as a reference (black lines) and those derived from the ERA5 data collocated with the GPS-RO observations. The red lines show diurnal cycles constructed from the collocated ERA5 data with daily and monthly mean removals in each 5° × 10° box while the blue lines show a raw composite. The latter poorly represents diurnal cycles in the polar regions because of the nonuniform local time sampling (Fig. 3) and high atmospheric variability there. The tropics are well approximated because of the low atmospheric variability. Over midlatitudes the raw collocated ERA5 results only roughly match the ERA5 diurnal cycle. After the daily and monthly mean removals, aliasing errors are almost eliminated (comparing red and black lines in Fig. 5). The largest error is ~0.075 K, occurring over the Southern Hemisphere polar region in JJA and SON seasons.

Although this study focuses on a TLS diurnal cycle climatology, the methods described above are also used to derive a climatology of diurnal cycles throughout the lower stratosphere from 300 to 10 hPa. Methods similarly follow those of Fig. 4, but instead of using TLS measurements we use temperature profiles.

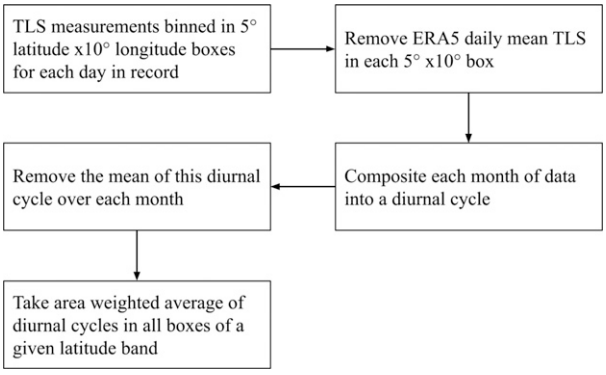

FIG. 4. Schematic figure describing the processing steps required to create the diurnal cycle climatology.

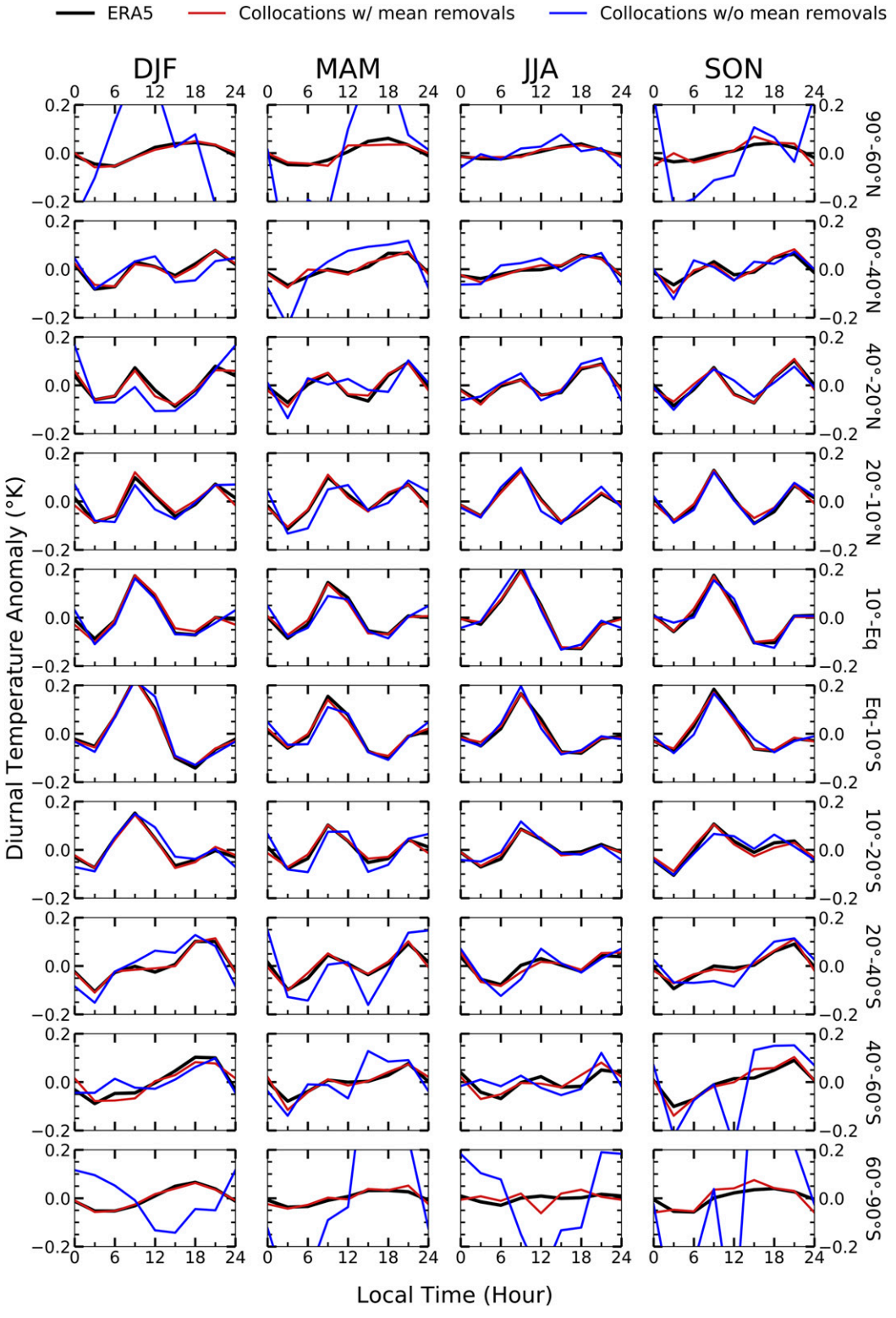

FIG. 5. Comparison of TLS diurnal cycles using all ERA5 data from March 2006–November 2020 (black), collocated ERA5 data with the GPS-RO observations after removing the ERA5 daily mean and monthly residual (red line), and without any mean removal (blue).

4. Results and discussion

TLS diurnal cycles based on GPS-RO observations in all zonal bands and all seasons are presented in Fig. 6 where we also provide the $\pm 2\sigma$ confidence interval for the diurnal anomaly at each zonal band in all seasons by performing a 10 000-iteration bootstrap on the monthly processed GPS-RO data. The Southern Hemisphere polar spring has the largest uncertainty in the diurnal cycle, likely due to the dearth of samples in this region during SON (see fourth panel in Fig. 3). The profiles of the diurnal cycles from 300 to 10 hPa are provided in Fig. 7. TLS diurnal temperature ranges are smaller than 0.4 K in all cases (Fig. 6). In Fig. 7, tropical diurnal cycles can reach amplitudes of ~1 K right above the tropopause and 1–2 K in the upper stratosphere due to the migrating tide (Xie et al. 2010; Khaykin et al. 2013). The stratospheric migrating tide is excited by absorption of solar radiation by ozone in the upper stratosphere (>30 hPa). The signature of this heating propagates downward with time leading to an increased migrating tide signature in the lower stratosphere (~50 hPa) which is about 9–12 h out of phase from that of the upper stratosphere, as evident in Fig. 7 (Zeng et al. 2008; Pirscher et al. 2010; Khaykin et al. 2013). The TLS weighting function covers both regions yet diurnal amplitudes are never larger than 0.4 K in any season. This is because the migrating tide of the upper stratosphere (>30 hPa) has its peak diurnal temperature from 18 to 24 and is in phase with the diurnal cycles of the upper troposphere (100–300 hPa) whereas the diurnal cycle near the tropical tropopause (100 hPa) reaches its minimum around the same time (Fig. 7). The diurnal cycle of the tropical tropopause is also influenced by the diurnal cycle of convection, leading to a diurnal cycle that is the result of both stratospheric and tropospheric processes (Khaykin et al. 2013). These dominant features dictate tropical upper-air diurnal temperature cycles thus may act to mute one another in the TLS diurnal cycle.

The lower-stratospheric temperature diurnal amplitudes are largest in the tropics (Figs. 6 and 7) and show some wave two structure in TLS (Fig. 6).The TLS diurnal cycles reach maximum amplitude in the summer season in the latitudinal band closest to the equator, as does the lower-stratospheric temperature near (above) 100 hPa, following the latitude of maximum convection. Further, these regions show the deepest late afternoon cold anomaly, pointing to the importance of deep convection on the lower-stratospheric temperature diurnal cycles (Dai and Trenberth 2004; Khaykin et al. 2013). This can be seen in Fig. 7 as a strong cold anomaly near 100 hPa in DJF from 0° to 10°S and JJA from 10°N to 0°.

The Arctic region is generally well captured by a wave one temperature diurnal cycle in all seasons. The upper stratosphere shows evidence of a weak migrating tide. Lower in the stratosphere the diurnal cycle amplitude is much smaller (Fig. 7). Although insolation does not change much in summer and winter Arctic, temperature diurnal cycles can still be driven by cloud presence and diurnal wind advection in polar regions (Barrigar 1963). Reanalysis and model simulations agree well with radio occultation derived MSU/AMSU TLS diurnal cycles in the Arctic (Fig. 6). Similarly, the Antarctic appears to have a weak migrating tide (Fig. 7, above 30 hPa). A slight wave two structure is present throughout the middle and lower stratosphere in the Antarctic during MAM, JJA, and SON (Fig. 7). This slight wave two structure is visible in the TLS diurnal cycles of these seasons but is not captured by reanalysis or model simulations (Fig. 6).

In all comparisons, model simulations and reanalysis do well at reproducing the observed range and phase of the diurnal cycles. Mean squared error (MSE) based on latitude and season is provided in Fig. 8. MSE is defined based on deviation from the GPS-RO TLS diurnal cycles. MSE is highest for both models and reanalysis in DJF. Across all seasons, MSE is largest in the tropics. CCM3 consistently performs the worst. WACCM6 has drastic updates in representation of the atmosphere compared to CCM3 as well as higher vertical resolution between 350 and 2 hPa, so its improvement is not surprising. Figure 8 also indicates that WACCM6 performs consistently better than ERA5 but only slightly.

Figure 9 shows the difference in diurnal anomalies between the ERA5 and GPS-RO climatology of diurnal cycles between 300 and 10 hPa. ERA5 bias is rarely above 0.2 K and is most evident as an overestimation of the diurnal anomaly associated with the migrating tide in the upper stratosphere. Lower in the stratosphere differences are smaller except for the tropical tropopause. In the tropics, differences between GPS-RO and ERA5 climatologies reach a local maximum near the tropical tropopause (~100 hPa). Because this region coincides with the peak of the TLS weighting function, it is likely this near-tropopause bias that accounts for the enhanced tropical MSE in Fig. 8.

To further characterize discrepancies between models/reanalysis and GPS-RO derived TLS diurnal cycles in the tropics (20°S–20°N), diurnal cycles over land and ocean for DJF and JJA separated by hemisphere are provided. Distinctions between land and ocean are provided in Fig. 10, and land/ocean TLS diurnal cycles are provided in Fig. 11. As previously mentioned, the largest diurnal cycles occur in the tropical summertime. This is particularly true for land, which exhibits the strongest afternoon cold anomaly. Other studies have attributed land-based late afternoon cold anomaly right above the tropical cold-point temperature (17 km) to deep convection, most prevalent during austral summertime (Khaykin et al. 2013). These temperature anomalies are likely driven by gravity waves propagating up and zonally away from deep convective source regions in South America and Africa (Sakazaki et al. 2015).

Liu and Zipser (2005) found the peak percentage of land-based deep convective features for 1400–1800 local time. This aligns with the minimum temperatures in the TLS diurnal cycles throughout much of the tropics (Fig. 6). The frequency of oceanic deep convection has a smaller diurnal cycle, which peaks in the early morning hours (Liu and Zipser 2005). We see little to no signature of additional early morning cooling in the summertime oceanic regions. We also see weaker but still obvious late afternoon cooling in the oceanic regions, suggesting land and ocean convection cannot alone describe the differences in the TLS diurnal cycles. Of course, attributing the features of the TLS diurnal cycle also needs to consider

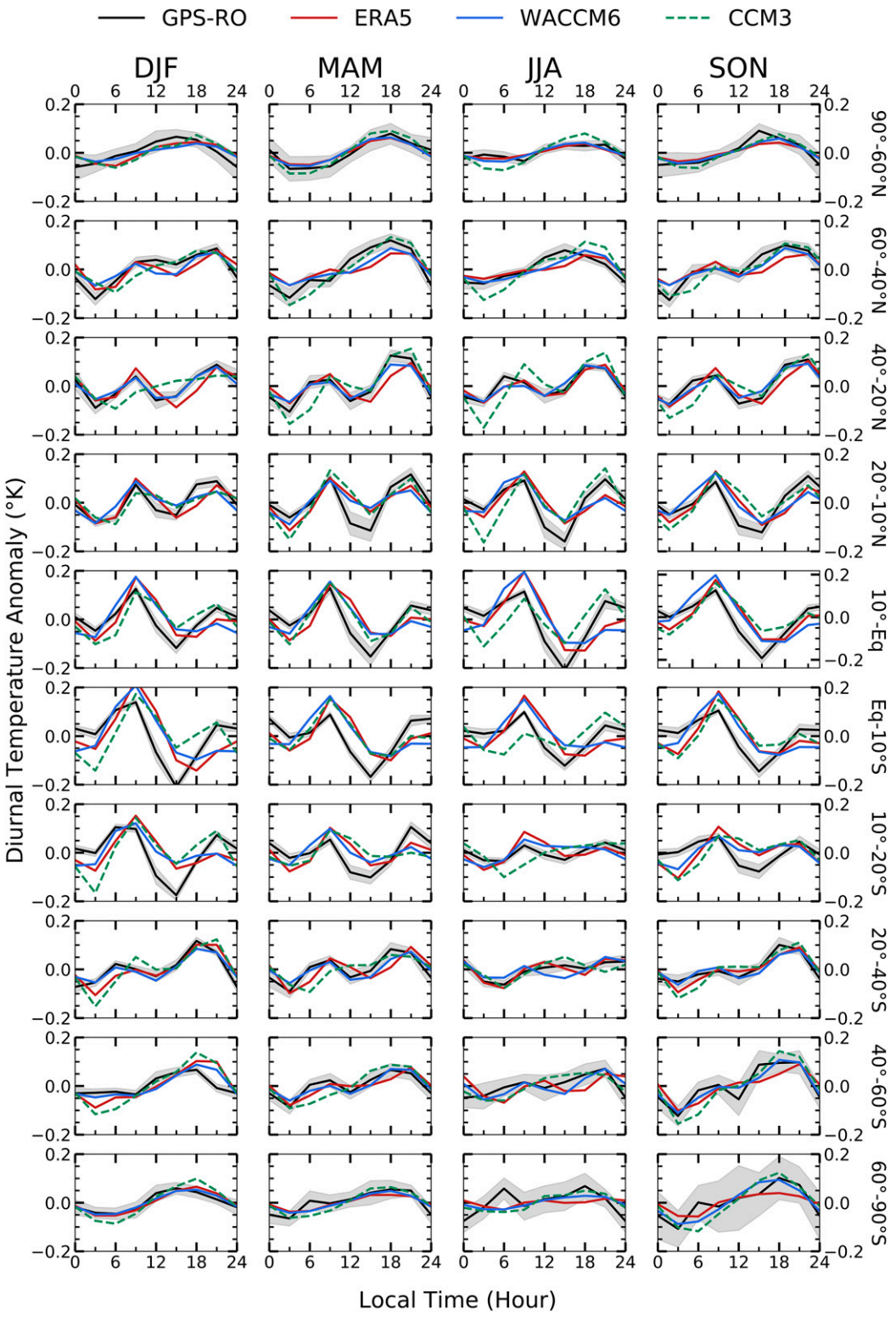

FIG. 6. TLS diurnal cycles observed from GPS-RO (black line), ERA5 (red line), WACCM6 (blue line), and CCM3 (dashed green line). Shading shows the $\pm 2\sigma$ confidence interval for the GPS-RO diurnal cycle.

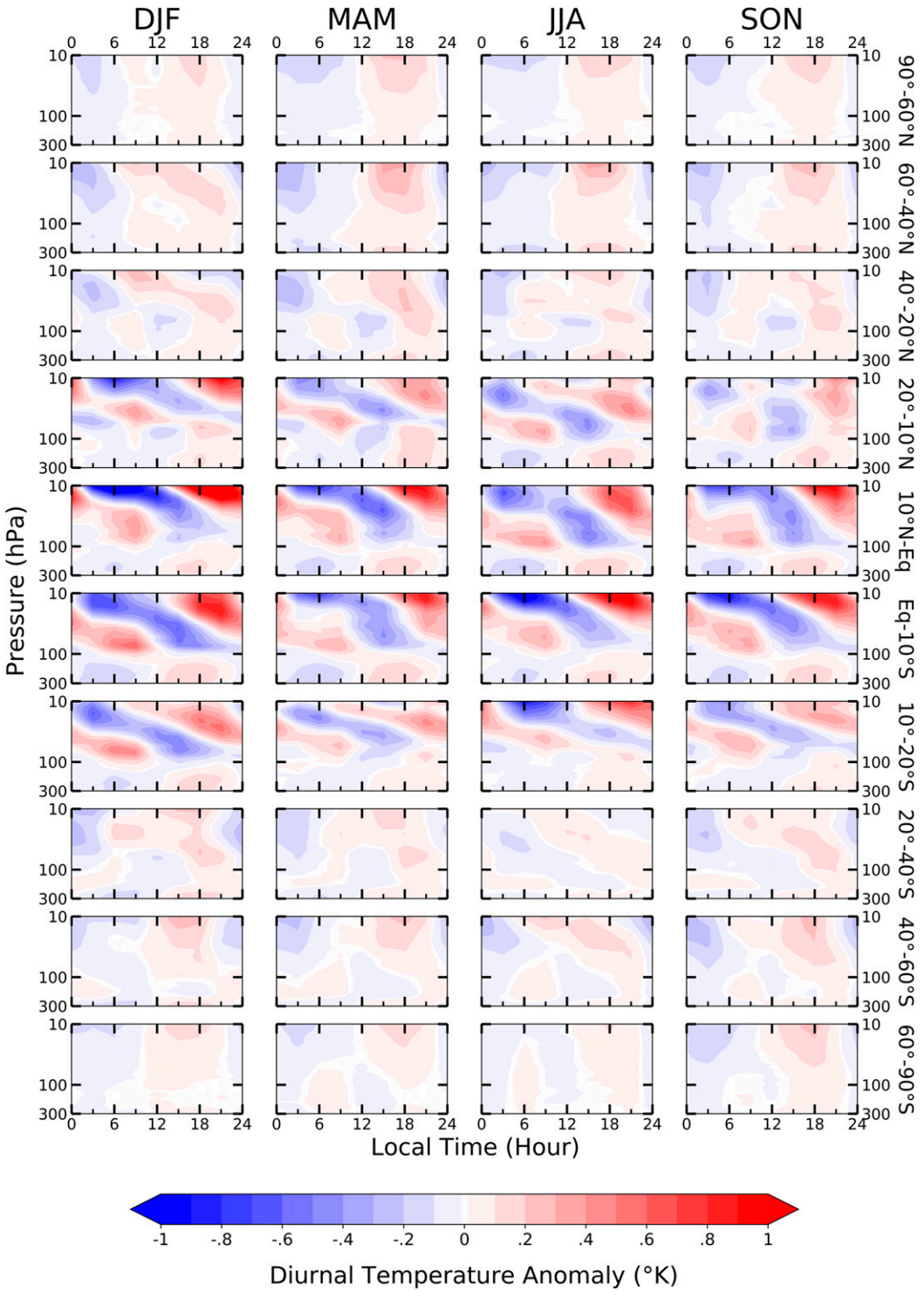

FIG. 7. Diurnal cycle profiles for 10 latitude bands and four seasons observed from GPS-RO. Contour intervals are 0.1 K. Diurnal anomalies smaller than ±0.01 K are white.

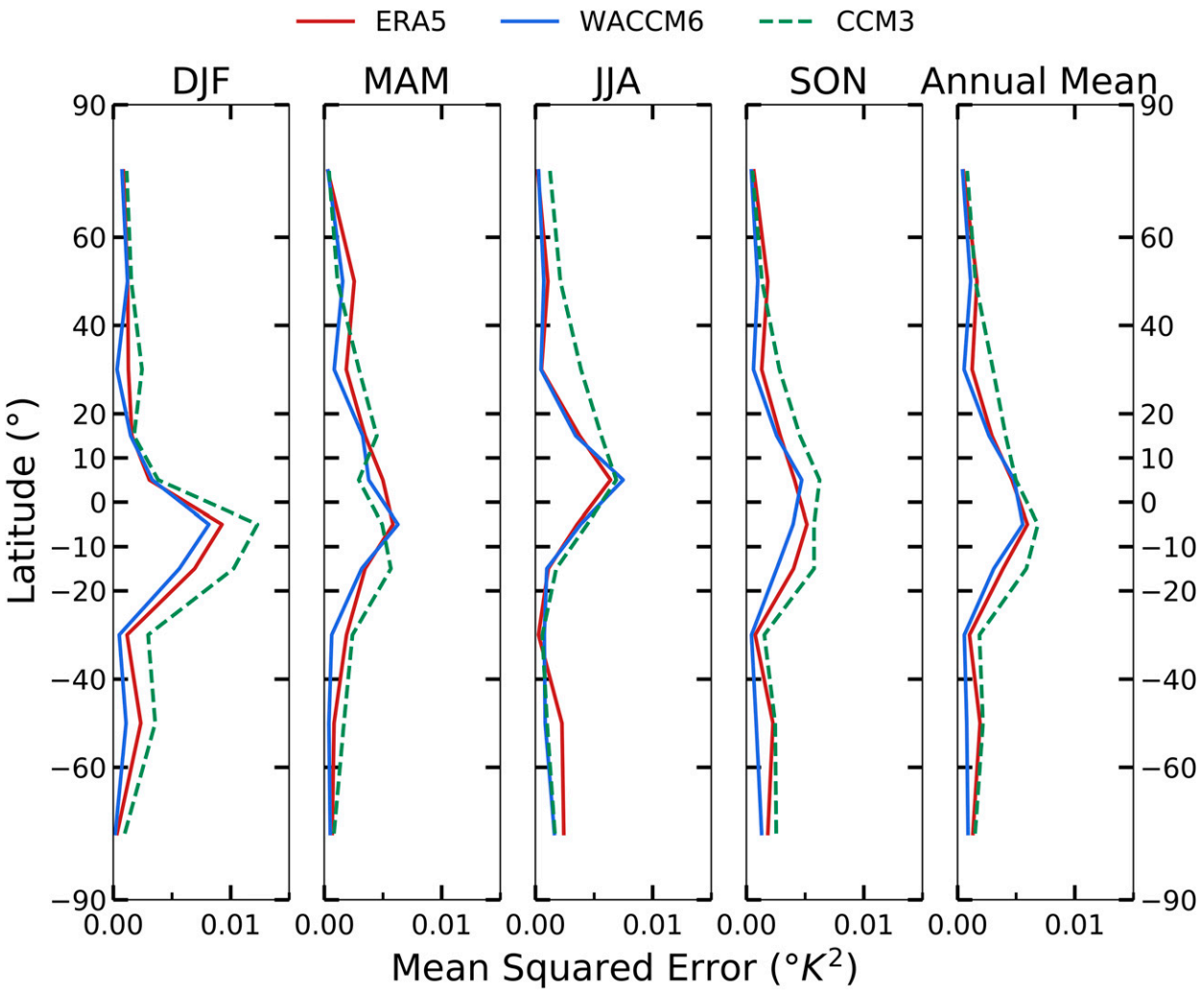

FIG. 8. Mean squared error of TLS diurnal cycles derived from model and reanalysis data as defined by deviation from GPS-RO diurnal cycles based on latitude and season.

the wide range of altitudes spanned by the TLS weighting function.

Models and reanalysis often overestimate the magnitude of the late morning/midday warm anomaly and underestimate the magnitude of the late afternoon cold anomaly in the tropics. Differences between model/reanalysis and GPS-RO data are largest around 1200 local time. It is interesting to note that ERA5 and WACCM6 show little disagreement (e.g., see DJF over 20°S–0° land in Fig. 11). Since we have confidence in the GPS-RO derived diurnal cycles over the tropics, there must be some common physical/dynamical processes near the tropical tropopause that are not represented well in both WACCM6 and ERA5. A similar ERA5 bias at heights near the tropical tropopause from 20°S to 20°N is visible in Fig. 9. Further research is needed in this aspect. Like the global results, CCM3 still tends to perform the worst. MSE is largest for both models and reanalysis in the austral summertime Southern Hemisphere land (Fig. 8).

5. Conclusions

Diurnal cycle climatologies are necessary to remove the effects of diurnal drift in satellite-based multidecadal climate records. Typically, this problem has been approached using GCMs due to the dearth of high-quality observationally based diurnal cycle climatologies in the TLS region. In this study we derived a GPS-RO based TLS diurnal cycle climatology, and a diurnal cycle climatology from 300 to 10 hPa. Sampling biases are reduced by taking advantage of the different orbital configurations provided by more than 14 years of data from 11 different satellites. Variability with time scales greater than one day are removed using daily mean data from ERA5. Bias incurred from this step is then removed over each month. The resulting climatology has high enough accuracy to resolve diurnal cycles with small diurnal temperature ranges over the whole globe. We then evaluated the quality of GCM simulation and reanalysis-based TLS diurnal cycle climatologies by comparing them to the GPS-RO data.

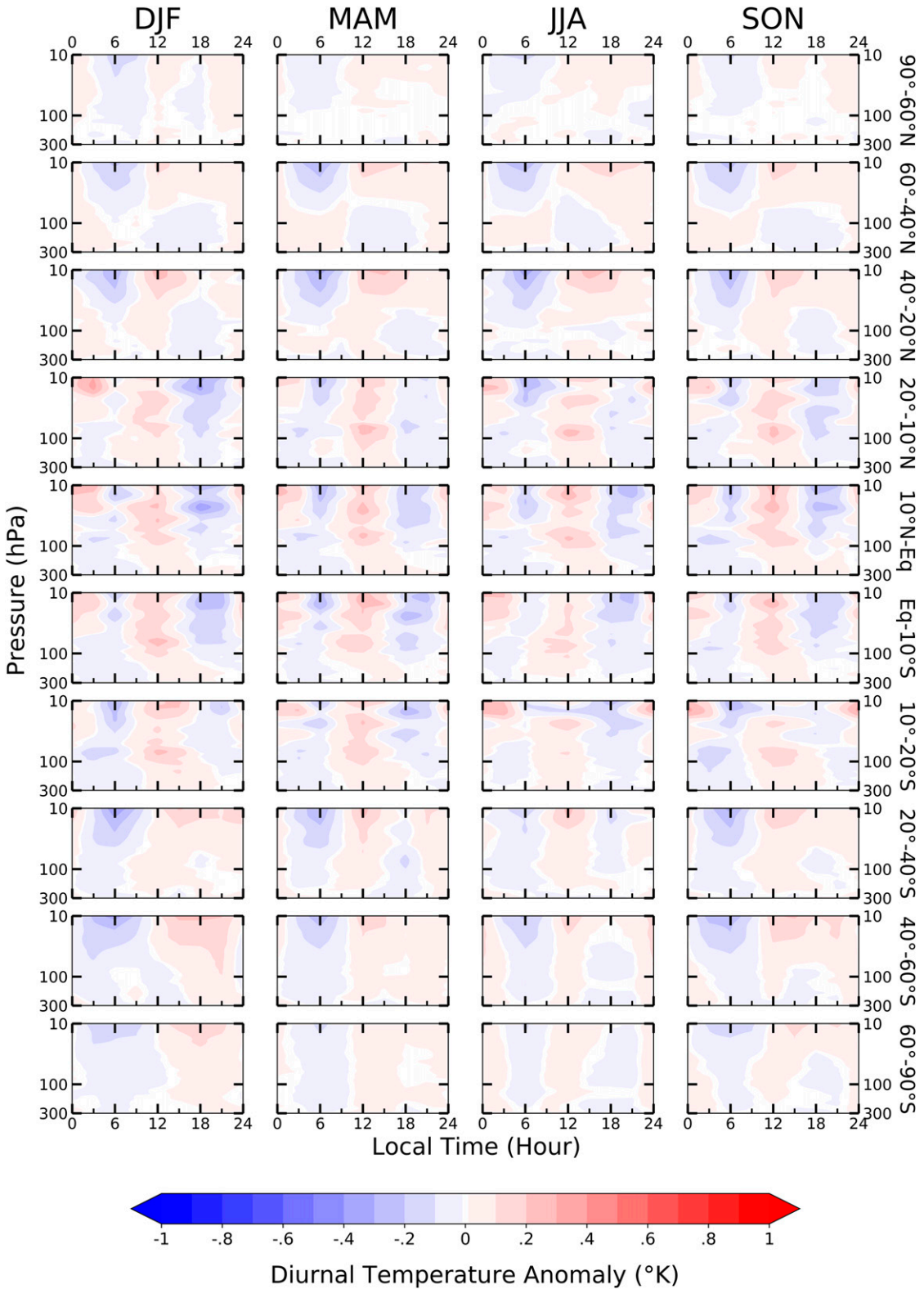

FIG. 9. Differences between ERA5 and GPS-RO diurnal climatology from 300 to 10 hPa. Differences are defined as ERA5 minus GPS-RO. Differences smaller than ±0.01 K are white.

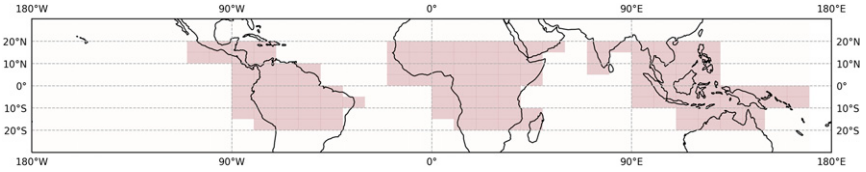

FIG. 10. Areas highlighted in red show land, defined for the comparison of land and ocean diurnal cycles from 20° equatorward.

Results of the GPS-RO climatology show TLS diurnal cycles over the globe are small with diurnal temperature ranges less than 0.4 K. The largest TLS diurnal cycles occur in the austral summertime over land. The smallest TLS diurnal cycles are in the polar summer and wintertime. Models and reanalysis data generally do well in reproducing diurnal temperature range and phase with the worst performance in the convective tropics during DJF.

In all seasons, MSE between model/reanalysis and GPS-RO observations TLS is largest in the tropics. A fault seen in both models and reanalysis was the underestimation of the late afternoon cold anomaly, and an overestimation of the midday warm anomaly in the tropics. The largest MSE occurs in the austral summertime tropics over the Southern Hemisphere. This region also experiences the largest TLS diurnal cycle with the deepest late afternoon cold anomaly. This points to the influence of deep convection on TLS diurnal cycles in this region. In the extratropics and polar regions, model and reanalysis data better match observed diurnal cycles.

ERA5 and WACCM6 perform better than the older CCM3 model in reproducing the TLS diurnal cycles. Ideally, diurnal corrections for the MSU/AMSU measurements could be applied based on our newly created observationally derived diurnal climatology. Because diurnal corrections are applied on horizontal scales of 2.5° latitude × 2.5° longitude the resolution required is higher than that attainable with the GPS-RO climatology. We thus suggest that future diurnal corrections of MSU/AMSU TLS measurements should rely on an updated diurnal cycle climatology provided by WACCM6 or ERA5 (which can achieve desired horizontal resolution), as opposed to the continued reliance on CCM3.

Acknowledgments. This research was supported by NASA Grant 80NSSC18K1031 and NSF Grant AGS-1821437. Radio occultation level 2 wetPrf data were provided by the COSMIC Data Analysis and Archive Center (CDAAC) at https://cdaac-www.cosmic.ucar.edu/. ERA5

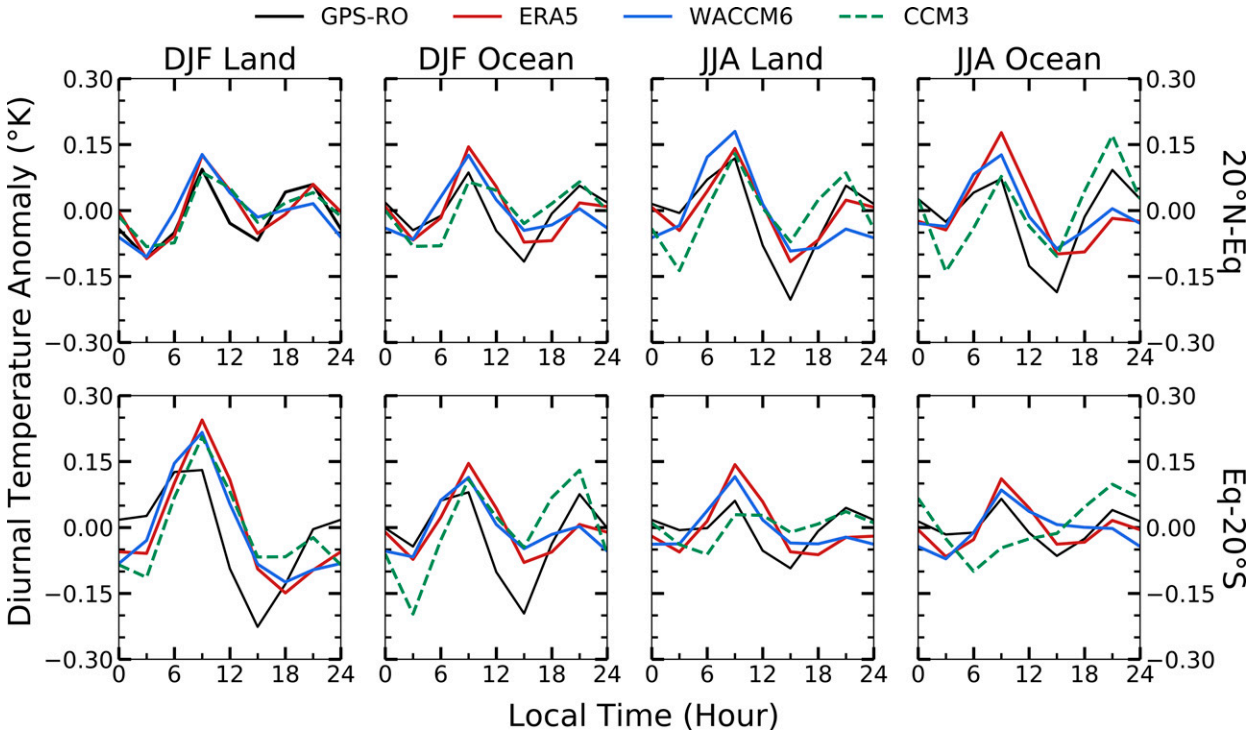

FIG. 11. TLS diurnal cycles of JJA and DJF seasons over tropical land and ocean in the (top) Northern Hemisphere and (bottom) Southern Hemisphere from GPS-RO (black line), ERA5 (red line), WACCM6 (blue line), and CCM3 (dashed green line).

hourly data on pressure levels were provided by the Copernicus Data Store at https://cds.climate.copernicus.eu/. WACCM6 Modern Climate simulations were run with the help of Mingcheng Wang from the University of Washington Department of Atmospheric Science on UCAR's Cheyenne computer. CCM3 data were provided by the Remote Sensing Systems RSS team and are available at ftp://ftp.remss.com/msu/data/diurnal_cycle/.

Data availability statement. Code and composites of diurnal cycles from both GPS-RO and ERA5 data after processing are available at https://github.com/AodhanSweeney.

REFERENCES

Anthes, R. A., 2011: Exploring Earth's atmosphere with radio occultation: Contributions to weather, climate and space weather. *Atmos. Meas. Tech.*, **4**, 1077–1103, https://doi.org/10.5194/amt-4-1077-2011.

——, and Coauthors, 2008: The COSMIC/FORMOSAT-3 mission: Early results. *Bull. Amer. Meteor. Soc.*, **89**, 313–334, https://doi.org/10.1175/BAMS-89-3-313.

Barrigar, D. B., 1963: A statistical investigation of the diurnal temperature variation during the polar night at McMurdo Sound, Antarctica. Naval Postgraduate School Rep., 94 pp., https://apps.dtic.mil/sti/citations/AD0413588.

Chapman, S., and R. S. Lindzen, 1970: *Atmospheric Tides.* Springer, 200 pp.

Christy, J. R., R. W. Spencer, and W. D. Braswell, 2000: MSU tropospheric temperatures: Dataset construction and radiosonde comparisons. *J. Atmos. Oceanic Technol.*, **17**, 1153–1170, https://doi.org/10.1175/1520-0426(2000)017<1153:MTTDCA>2.0.CO;2.

Dai, A., and K. E. Trenberth, 2004: The diurnal cycle and its depiction in the Community Climate System Model. *J. Climate*, **17**, 930–951, https://doi.org/10.1175/1520-0442(2004)017<0930:TDCAID>2.0.CO;2.

Das, U., W. E. Ward, C. J. Pan, and S. K. Das, 2020: Migrating and non-migrating tides observed in the stratosphere from FORMOSAT-3/COSMIC temperature retrievals. *Ann. Geophys.*, **38**, 421–435, https://doi.org/10.5194/angeo-38-421-2020.

Fu, Q., and C. M. Johanson, 2004: Stratospheric influences on MSU-derived tropospheric temperature trends: A direct error analysis. *J. Climate*, **17**, 4636–4640, https://doi.org/10.1175/JCLI-3267.1.

——, and ——, 2005: Satellite-derived vertical dependence of tropical tropospheric temperature trends. *Geophys. Res. Lett.*, **32**, L10703, https://doi.org/10.1029/2004GL022266.

——, and P. Lin, 2011: Poleward shift of subtropical jets inferred from satellite-observed lower-stratospheric temperatures. *J. Climate*, **24**, 5597–5603, https://doi.org/10.1175/JCLI-D-11-00027.1.

——, C. M. Johanson, S. G. Warren, and D. J. Seidel, 2004: Contribution of stratospheric cooling to satellite-inferred tropospheric temperature trends. *Nature*, **429**, 55–58, https://doi.org/10.1038/nature02524.

——, ——, J. M. Wallace, and T. Reichler, 2006: Enhanced midlatitude tropospheric warming in satellite measurements. *Science*, **312**, 1179, https://doi.org/10.1126/science.1125566.

——, S. Solomon, and P. Lin, 2010: On the seasonal dependence of tropical lower-stratospheric temperature trends. *Atmos. Chem. Phys.*, **10**, 2643–2653, https://doi.org/10.5194/acp-10-2643-2010.

——, S. Manabe, and C. M. Johanson, 2011: On the warming in the tropical upper troposphere: Models versus observations. *Geophys. Res. Lett.*, **38**, L15704, https://doi.org/10.1029/2011GL048101.

——, R. H. White, M. Wang, B. Alexander, S. Solomon, A. Gettelman, D. S. Battisti, and P. Lin, 2020: The Brewer-Dobson circulation during the Last Glacial Maximum. *Geophys. Res. Lett.*, **47**, e2019GL086271, https://doi.org/10.1029/2019GL086271.

Gettelman, A., and Coauthors, 2019: The Whole Atmosphere Community Climate Model version 6 (WACCM6). *J. Geophys. Res. Atmos.*, **124**, 12 380–12 403, https://doi.org/10.1029/2019JD030943.

He, W., S. Ho, H. Chen, X. Zhou, D. Hunt, and Y.-H. Kuo, 2009: Assessment of radiosonde temperature measurements in the upper troposphere and lower stratosphere using COSMIC radio occultation data. *Geophys. Res. Lett.*, **36**, L17807, https://doi.org/10.1029/2009GL038712.

Hersbach, H., and Coauthors, 2020: The ERA5 global reanalysis. *Quart. J. Roy. Meteor. Soc.*, **146**, 1999–2049, https://doi.org/10.1002/qj.3803.

Ho, S., M. Goldberg, Y.-H. Kuo, C.-Z. Zou, and W. S. Schreiner, 2009: Calibration of temperature in the lower stratosphere from microwave measurements using COSMIC radio occultation data: Preliminary results. *Terr. Atmos. Oceanic Sci.*, **20**, 87–100, https://doi.org/10.3319/TAO.2007.12.06.01(F3C).

Johnston, B. R., F. Xie, and C. Liu, 2018: The effects of deep convection on regional temperature structure in the tropical upper troposphere and lower stratosphere. *J. Geophys. Res. Atmos.*, **123**, 1585–1603, https://doi.org/10.1002/2017JD027120.

Kennedy, J. J., P. Brohan, and S. F. B. Tett, 2007: A global climatology of the diurnal variations in sea-surface temperature and implications for MSU temperature trends. *Geophys. Res. Lett.*, **34**, L05712, https://doi.org/10.1029/2006GL028920.

Khaykin, S. M., J.-P. Pommereau, and A. Hauchecorne, 2013: Impact of land convection on temperature diurnal variation in the tropical lower stratosphere inferred from COSMIC GPS radio occultations. *Atmos. Chem. Phys.*, **13**, 6391–6402, https://doi.org/10.5194/acp-13-6391-2013.

Kuo, Y.-H., T.-K. Wee, S. Sokolovskiy, C. Rocken, W. Schreiner, D. Hunt, and R. A. Anthes, 2004: Inversion and error estimation of GPS radio occultation data. *J. Meteor. Soc. Japan*, **82**, 507–531, https://doi.org/10.2151/jmsj.2004.507.

Kursinski, E. R., G. A. Hajj, J. T. Schofield, R. P. Linfield, and K. R. Hardy, 1997: Observing Earth's atmosphere with radio occultation measurements using the global positioning system. *J. Geophys. Res.*, **102**, 23 429–23 465, https://doi.org/10.1029/97JD01569.

Liu, C., and E. J. Zipser, 2005: Global distribution of convection penetrating the tropical tropopause. *J. Geophys. Res.*, **110**, D23104, https://doi.org/10.1029/2005JD006063.

Mears, C. A., and F. J. Wentz, 2005: The effect of diurnal correction on satellite-derived lower tropospheric temperature. *Science*, **309**, 1548–1551, https://doi.org/10.1126/science.1114772.

——, and ——, 2009: Construction of the remote sensing systems V3.2 atmospheric temperature records from the MSU and AMSU microwave sounders. *J. Atmos. Oceanic Technol.*, **26**, 1040–1056, https://doi.org/10.1175/2008JTECHA1176.1.

——, and ——, 2016: Sensitivity of satellite-derived tropospheric temperature trends to the diurnal cycle adjustment. *J. Climate*, **29**, 3629–3646, https://doi.org/10.1175/JCLI-D-15-0744.1.

——, M. C. Schabel, F. J. Wentz, B. D. Santer, and B. Govindasamy, 2002: Correcting the MSU middle tropospheric temperature for diurnal drifts. *IEEE Int. Geoscience and Remote Sensing Symp.*, Toronto, ON, Canada, IEEE, 1839–1841, https://doi.org/10.1109/IGARSS.2002.1026272.

——, ——, and ——, 2003: A reanalysis of the MSU channel 2 tropospheric temperature record. *J. Climate*, **16**, 3650–3664, https://doi.org/10.1175/1520-0442(2003)016<3650:AROTMC>2.0.CO;2.

——, F. J. Wentz, P. Thorne, and D. Bernie, 2011: Assessing uncertainty in estimates of atmospheric temperature changes from MSU and AMSU using a Monte-Carlo estimation technique. *J. Geophys. Res.*, **116**, D08112, https://doi.org/10.1029/2010JD014954.

Pirscher, B., U. Foelsche, B. C. Lackner, and G. Kirchengast, 2007: Local time influence in single-satellite radio occultation climatologies from sun-synchronous and non-sun-synchronous satellites. *J. Geophys. Res.*, **112**, D11119, https://doi.org/10.1029/2006JD007934.

——, ——, M. Borsche, G. Kirchengast, and Y.-H. Kuo, 2010: Analysis of migrating diurnal tides detected in FORMOSAT-3/COSMIC temperature data. *J. Geophys. Res.*, **115**, D14108, https://doi.org/10.1029/2009JD013008.

Po-Chedley, S., T. J. Thorsen, and Q. Fu, 2015: Removing diurnal cycle contamination in satellite-derived tropospheric temperatures: Understanding tropical tropospheric trend discrepancies. *J. Climate*, **28**, 2274–2290, https://doi.org/10.1175/JCLI-D-13-00767.1.

——, B. D. Santer, S. Fueglistaler, M. D. Zelinka, P. J. Cameron-Smith, J. F. Painter, and Q. Fu, 2021: Natural variability contributes to model–satellite differences in tropical tropospheric warming. *Proc. Natl. Acad. Sci. USA*, **118**, e2020962118, https://doi.org/10.1073/pnas.2020962118.

Sakazaki, T., K. Sato, Y. Kawatani, and S. Watanabe, 2015: Three-dimensional structures of tropical nonmigrating tides in a high-vertical-resolution general circulation model. *J. Geophys. Res. Atmos.*, **120**, 1759–1775, https://doi.org/10.1002/2014JD022464.

Santer, B. D., and Coauthors, 2017: Comparing tropospheric warming in climate models and satellite data. *J. Climate*, **30**, 373–392, https://doi.org/10.1175/JCLI-D-16-0333.1.

——, and Coauthors, 2019: Celebrating the anniversary of three key events in climate change science. *Nat. Climate Change*, **9**, 180–182, https://doi.org/10.1038/s41558-019-0424-x.

Seidel, D. J., M. Free, and J. Wang, 2005: Diurnal cycle of upper-air temperature estimated from radiosondes. *J. Geophys. Res.*, **110**, D09102, https://doi.org/10.1029/2004JD005526.

Simmons, A., and Coauthors, 2020: Global stratospheric temperature bias and other stratospheric aspects of ERA5 and ERA5.1. ECMWF Tech. Memo. 859, 40 pp., https://doi.org/10.21957/rcxqfmg0.

Suneeth, K. V., S. Das, and S. Das, 2017: Diurnal variability of the global tropical tropopause: Results inferred from COSMIC observations. *Climate Dyn.*, **49**, 3277–3292, https://doi.org/10.1007/s00382-016-3512-x.

Wentz, F. J., and M. Schabel, 1998: Effects of orbital decay on satellite-derived lower-tropospheric temperature trends. *Nature*, **394**, 661–664, https://doi.org/10.1038/29267.

Xie, F., D. L. Wu, C. O. Ao, and A. J. Mannucci, 2010: Atmospheric diurnal variations observed with GPS radio occultation soundings. *Atmos. Chem. Phys.*, **10**, 6889–6899, https://doi.org/10.5194/acp-10-6889-2010.

Young, P. J., K. H. Rosenlof, S. Solomon, S. C. Sherwood, Q. Fu, and J.-F. Lamarque, 2012: Changes in stratospheric temperatures and their implications for changes in the Brewer–Dobson circulation, 1979–2005. *J. Climate*, **25**, 1759–1772, https://doi.org/10.1175/2011JCLI4048.1.

Zeng, Z., W. Randel, S. Sokolovskiy, C. Deser, Y.-H. Kuo, M. Hagan, J. Du, and W. Ward, 2008: Detection of migrating diurnal tide in the tropical upper troposphere and lower stratosphere using the Challenging Minisatellite Payload radio occultation data. *J. Geophys. Res.*, **113**, D03102, https://doi.org/10.1029/2007JD008725.

——, S. Sokolovskiy, W. S. Schreiner, and D. Hunt, 2019: Representation of vertical atmospheric structures by radio occultation observations in the upper troposphere and lower stratosphere: Comparison to high-resolution radiosonde profiles. *J. Atmos. Oceanic Technol.*, **36**, 655–670, https://doi.org/10.1175/JTECH-D-18-0105.1.

Zou, C.-Z., and W. Wang, 2009: Diurnal drift correction in the NESDIS/STAR MSU/AMSU atmospheric temperature climate data record. *Proc. SPIE*, **7456**, 74560G, https://doi.org/10.1117/12.824459.